

Chapter 2

DUNE

The Deep Underground Neutrino Experiment (DUNE) will be a new generation world-leading Long Baseline oscillation experiment. Among its main goals are the precise measurement of the oscillation parameters, the study of matter-antimatter asymmetry and the determination of the neutrino mass ordering. It is conceived around three main components: The NuMi neutrino Beam, which is able to produce an intense and wide muon neutrino and antineutrino band; a fine-grained Near Detector (ND) situated at the Fermi National Accelerator Laboratories (Fermilab, Batavia, Illinois), just downstream of the neutrino source; a massive Liquid Argon Time Projection Chamber (LArTPC) Far Detector (FD) placed 1300 km downstream at the Sanford Underground Research Facility (Lead, South Dakota).

In this chapter we will discuss DUNE’s physics programme (Section 1) as well as the configuration of the neutrino beam and its main detectors (Section 3). KLOE, which is one of DUNE’s Near Detectors and the subject of the simulations performed for this thesis will be discussed more in detail in the next chapter.

2.1 DUNE’s scientific program

The scientific objectives of DUNE are categorized into a *primary* and an *ancillary* scientific programme [46]. The latter is further divided into secondary objectives that could be pursued by the experiment just by virtue of how it will be built and additional secondary objectives that may require specific upgrades to the facility.

The *primary* programme is made up by the main measurements that DUNE will be built to perform with unprecedented precision which coincide with the fundamental questions that this experiment will try to answer:

1. **Measurement of the charge-parity violating phase δ_{CP} and determination of the mass ordering of the neutrinos** (i.e. the sign of $\Delta m_{31} = m_3^2 - m_1^2$). The study of δ_{CP} is particularly important in cosmological models trying to explain the matter-antimatter asymmetry in the universe.
2. **Precision measurements of the $\nu_\mu \rightarrow \nu_{\mu,e}$ oscillation parameters:** the θ_{13} mixing angle; the θ_{23} mixing angle and the octant it lies in; the value of the $|\Delta m_{32}^2|$ mass difference. Precision measurements of these parameters and comparisons with corresponding patterns in the quark sector will further our knowledge of the underlying symmetries in fundamental particle physics.
3. **Search for proton decay in one or more decay modes, improving significantly on previous lifetime limits.** Most Grand Unified Theories (GUTs) make lifetime predictions for nucleons and putting more and more stringent limits will be fundamental in assessing which one of them might be correct.
4. **Detection and measurements of the neutrino flux from a core-collapse supernova.** In particular the time structure and energy spectrum of the neutrino burst would much further our understanding of this astrophysical phenomenon.

The *ancillary* programme consists of objectives that DUNE is not specifically conceived to achieve, but that are nonetheless enabled by the facility's design.:

1. Further accelerator oscillation measurements and search for non-standard interactions beyond the standard model (BSD)
2. Atmospheric neutrino oscillation measurements
3. Measurements of other astrophysical phenomena using moderate energy neutrinos

Finally the *additional secondary* programme includes measurements potentially made possible by future upgrades to the facility such as monitoring of the diffuse supernova flux, solar neutrino and other low energy astrophysical neutrino measurements.

The high granularity and precision required by the *DUNE Near Detector (ND)* will also allow it to have a scientific programme of its own. Its main objective will be to perform all the precision measurements necessary to

achieve the goals of the primary programme. It will also pursue precision studies of the weak interaction, studies of nuclear and nucleon structure and searches for new physics (discussed more in detail in Chapter 3).

2.1.1 Sensitivities and systematics

In order to make any precision measurement one should be acutely aware of the systematic uncertainties related to the analysis strategy and the performance of the detector. In a two detectors Long Baseline experiment the ν_μ spectrum measured in the Near Detector $N_{ND}^{data}(\nu_\mu)$ is propagated to the Far Detector and is used to predict the expected signal of ν_μ and oscillated ν_e (and much smaller component of oscillated ν_τ) i.e. $N_{FD}^{exp}(\nu_\mu)$ and $N_{FD}^{exp}(\nu_e)$. Likewise the ν_e measured spectrum in the ND, mostly comprised of electron neutrinos from the beam and misidentified NC π^0 is used to predict the background at the FD.

The measured neutrino spectrum at the near detector is given by:

$$N_{ND}^{data}(\nu_{\mu,e}) = \Phi_{ND}(\nu_{\mu,e}) \otimes \varepsilon_{ND}(\nu_{\mu,e}) \otimes \sigma_{ND}(\nu_{\mu,e}) \quad (2.1)$$

where $\Phi_{ND}(\nu_{\mu,e})$ is the beam flux, $\varepsilon_{ND}(\nu_{\mu,e})$ is the detector's efficiency and $\sigma_{ND}(\nu_{\mu,e})$ is the neutrino interaction cross section. In order to use such data to predict the signal and background expected at the far detector one needs to take into consideration:

- *Differences in how the neutrino interact* σ_{FD}/σ_{ND} . These are null in the case that the target nuclei in the Near and Far Detector are the same. Otherwise the dominating uncertainties in the prediction of ν_e in FD from measurement of ν_μ in ND are the ones arising from differences in the electronic and muonic cross sections between the detectors: $\sigma_{FD}(\nu_e)/\sigma_{ND}(\nu_\mu)$.
- *Differences in detector efficiencies* $\varepsilon_{FD}/\varepsilon_{ND}$. These uncertainties mostly arise from the differences in event selection between the two detectors and in particular the modelling of the energy scales. These are also virtually nonexistent in the case that ND and FD are identical.
- *Differences in the neutrino flux* Φ_{FD}/Φ_{ND} . The fluxes at the Near and Far detector are radically different since the ND is very close to the beamline and sees an expended source, while the FD is 1300 km away. A Monte Carlo is used to simulate the beam propagation, but it is itself not immune from inaccuracies: errors in the hadron production, focusing of the horns composition of the beam pipe and decay channel geometry can all contribute.

Source of Uncertainty	MINOS Absolute/ ν_e	T2K ν_e	LBNE ν_e	Comments
Beam Flux after N/F extrapolation	3%/0.3%	2.9%	2%	MINOS is normalization only. LBNE normalization and shape highly correlated between ν_μ/ν_e .
Detector effects				
Energy scale (ν_μ)	7%/3.5%	included above	(2%)	Included in LBNE ν_μ sample uncertainty only in three-flavor fit. MINOS dominated by hadronic scale.
Absolute energy scale (ν_e)	5.7%/2.7%	3.4% includes all FD effects	2%	Totally active LArTPC with calibration and test beam data lowers uncertainty.
Fiducial volume	2.4%/2.4%	1%	1%	Larger detectors = smaller uncertainty.
Neutrino interaction modeling				
Simulation includes: hadronization cross sections nuclear models	2.7%/2.7%	7.5%	$\sim 2\%$	Hadronization models are better constrained in the LBNE LArTPC. N/F cancellation larger in MINOS/LBNE. X-section uncertainties larger at T2K energies. Spectral analysis in LBNE provides extra constraint.
Total	5.7%	8.8%	3.6 %	Uncorrelated ν_e uncertainty in full LBNE three-flavor fit = 1-2%.

Table 2.1: Dominant systematics on the ν_e appearance channel for T2K and MINOS and projection for LBNE (Long Baseline Neutrino Experiment), the preliminary name used for DUNE [46]

Taking all of this into consideration one can then use neutrinos' oscillation and survival probability in order to predict the muonic and electronic signal in the Far Detector. The ν_μ expected signal is given by:

$$N_{FD}^{exp}(\nu_\mu) = N_{ND}^{data}(\nu_\mu) \otimes \frac{\Phi_{FD}(\nu_\mu)}{\Phi_{ND}(\nu_\mu)} \otimes P(\nu_\mu \rightarrow \nu_\mu) \otimes \frac{\varepsilon_{FD}(\nu_\mu)}{\varepsilon_{ND}(\nu_\mu)} \otimes \frac{\sigma_{FD}(\nu_\mu)}{\sigma_{ND}(\nu_\mu)} \quad (2.2)$$

The ν_e expected signal is given by:

$$\begin{aligned} N_{FD}^{exp}(\nu_\mu) &= N_{ND}^{data}(\nu_\mu) \otimes \underbrace{\frac{\Phi_{FD}(\nu_\mu)}{\Phi_{ND}(\nu_\mu)} \otimes P(\nu_\mu \rightarrow \nu_e) \otimes \frac{\varepsilon_{FD}(\nu_e)}{\varepsilon_{ND}(\nu_\mu)} \otimes \frac{\sigma_{FD}(\nu_e)}{\sigma_{ND}(\nu_\mu)}}_{\text{Expected signal}} \\ &+ N_{ND}^{data}(\nu_e) \otimes \underbrace{\frac{\Phi_{FD}(\nu_e)}{\Phi_{ND}(\nu_e)} \otimes P(\nu_e \rightarrow \nu_e) \otimes \frac{\varepsilon_{FD}(\nu_e)}{\varepsilon_{ND}(\nu_e)} \otimes \frac{\sigma_{FD}(\nu_e)}{\sigma_{ND}(\nu_e)}}_{\text{Electronic events from the beam}} \\ &+ \pi^0 \text{NC background prediction from } N_{ND}^{data}(\nu_e) \\ &+ \nu_\tau \text{ background prediction from } N_{ND}^{data}(\nu_\mu) \end{aligned} \quad (2.3)$$

The main sources of uncertainties are well known from previous experiments such as T2K and MINOS. They include:

- *Beam flux uncertainties*: related to the precision with which the ND is capable to measure the unoscillated beam flux in both shape and normalization.
- *ν_μ energy-scale uncertainties*: the muonic neutrino energy spectrum measured in the ND is then used to predict the ν_e appearance channel in the FD and the energy scale uncertainty scale is thus propagated.
- *Absolute ν_e energy-scale uncertainty*: an accurate measurement of the shape of the ν_e appearance channel is essential to oscillation sensitivity and depends on how well the detector response is understood
- *Simulation uncertainties*: uncertainties related to the modelling of the neutrino interactions with the target nuclei in the near and far detectors.

In Table 2.1 the dominant uncertainties for ν_e appearance for the T2K and MINOS and a preliminary prediction for DUNE are summarized. The precision is expected to improve from all fronts.

2.1.2 Mass ordering and δ_{CP}

As it can be seen from Eq. 1.49 both a non-zero δ_{CP} and matter effects can induce asymmetries between $P(\nu_\mu \rightarrow \nu_e)$ and $P(\bar{\nu}_\mu \rightarrow \bar{\nu}_e)$ and thus:

$$\mathcal{A}_{CP} = \mathcal{A}_\delta + \mathcal{A}_{matter} \quad (2.4)$$

In figure 2.2 the asymmetries induced by CP violation (\mathcal{A}_δ) in case that $\delta_{CP} = \pm\pi/2$ and by matter effects (\mathcal{A}_{matter}) are plotted separately in 2d oscillograms as a function of baseline and Energy. In reality though the two asymmetries always operate at the same time if δ_{CP} is not null and the matter effects are not trivial. In experiments where both are relevant then, if one wants to use measurements of total asymmetry both to measure δ_{CP} and the mass ordering, then it's mandatory to be able to disambiguate between the two [47].

For the MSW effects in particular the asymmetries are introduced by a CP violating term $P_{\sin \delta}$ in the oscillation probability:

$$P(\nu_\mu \rightarrow \nu_e) \simeq P(\nu_e \rightarrow \nu_\mu) \simeq P_0 + P_{\sin \delta} + P_{\cos \delta} + P_3 \quad (2.5)$$

where

$$P_0 = \sin^2 \theta_{23} \frac{\sin^2 2\theta_{13}}{(A - 1)^2} \sin^2[(A - 1)\Delta] \quad (2.6)$$

$$P_3 = \alpha^2 \cos^2 \theta_{13} \frac{\sin^2 2\theta_{12}}{A^2} \sin^2(A\Delta) \quad (2.7)$$

$$P_{\sin \delta} = \alpha \frac{8J_{CP}}{A(1-A)} \sin \Delta \sin(\Delta A) \sin((1-A)\Delta) \quad (2.8)$$

$$P_{\cos \delta} = \alpha \frac{8J_{CP} \cot \delta_{CP}}{A(1-A)} \sin \Delta \sin(\Delta A) \sin((1-A)\Delta) \quad (2.9)$$

with

$$\Delta = \Delta m_{31}^2 L / 4E \quad (2.10)$$

$$A = \sqrt{3} G_F N_e 2E / \Delta m_{31}^2 \quad (2.11)$$

$$\alpha = |\Delta m_{12}^2| / |\Delta m_{31}^2| \quad (2.12)$$

Note that since the value of Δm_{31}^2 switches between normal and inverted hierarchy, the asymmetry effects induced by the passage through matter will also be different: for normal (inverted) hierarchy $P(\nu_\mu - \nu_e)$ is enhanced (suppressed) and $P(\bar{\nu}_\mu - \bar{\nu}_e)$ is suppressed (enhanced); the matter effects shift the phase of oscillation pattern for a fixed baseline to lower energies (by about -100 MeV) in the IH.

In general the matter effects have the largest impacts when the oscillation nodes for θ_{13} are reached (the first two nodes are highlighted in black in Fig. 2.2):

$$\frac{L(\text{km})}{E(\text{GeV})} = (2n-1) \frac{\pi}{2} \frac{1}{(1.27 \times \Delta m_{31}^2 (\text{eV}^2))} \simeq (2n-1) \times 510 \text{km/GeV} \quad (2.13)$$

For an experiment such as DUNE, where we have a baseline of $L \sim 1300 \text{ km}$ (highlighted in black in Fig. 2.2) and an energy range $E \sim 5 - 10 \text{ GeV}$, the matter effects are maximal, and it is then crucial that they are disentangled from the CP effects.

Knowing the value of $|\Delta m_{31}^2|$ (only the sign is still unknown), one can see, though, that for a baseline $> 1200 \text{ km}$, the size of $\mathcal{A}_{\text{matter}}$ surpasses the highest possible value of \mathcal{A}_δ which makes the disambiguation between the two effects possible. In Figure the plots show the total asymmetry at the first (black) and second (red) as a function of δ_{CP} for four different values of L : 290km, 810km, 1300km (baseline of DUNE) and 2300km. The NH and IH the total asymmetries will have different values because of the matter effects and are plotted as full and dashed lines respectively. As the baseline gets bigger, given the same node, the CP-induced asymmetry will stay the same while matter induced one will get bigger since the dependencies on L and E are:

$$\mathcal{A}_\delta \propto L/E \quad (2.14)$$

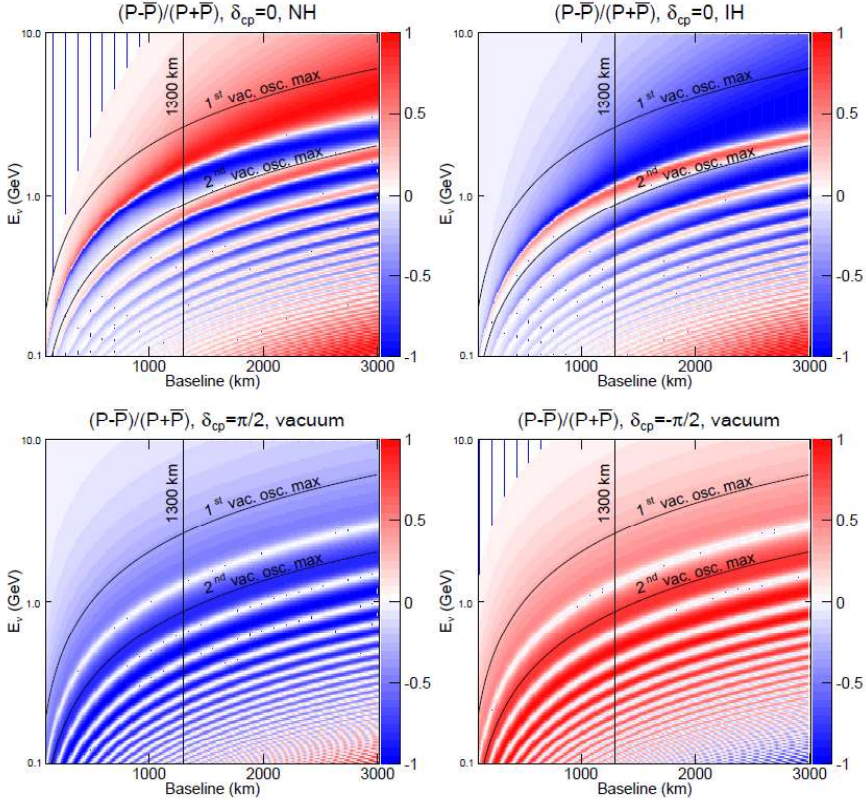


Figure 2.2: \mathcal{A}_{CP} total asymmetry as a function of baseline and energy. The top two oscillograms show the asymmetry for $\delta_{CP} = 0$ (i.e. \mathcal{A}_{matter}) for Normal(left) and Inverted (right) mass ordering. The two bottom oscillograms show the asymmetry in vacuum (i.e. \mathcal{A}_δ) for $\delta_{CP} = \pi/2$ (left) and $\delta_{CP} = -\pi/2$ (right). DUNE’s baseline (1300km) and the 1st and 2nd oscillation nodes are highlighted in black. [47]

$$\mathcal{A}_{matter} \propto L \times E \quad (2.15)$$

If one considers then the case in which the δ_{CP} asymmetries is maximal (green line in the plots) is easy to see that if $\mathcal{A}_{matter} < \mathcal{A}_\delta(\max)$ the same total asymmetry is compatible with both hierarchies and multiple value of δ_{CP} . This is true for baselines shorter than 1200km. For DUNE, where $L \sim 1300\text{km}$ these ambiguities don’t exist.

Significance for mass ordering and δ_{CP} measurements

The sensitivity with which the DUNE experiment will be able to measure the mass ordering (MO) and CP-Violation (CPV), is evaluated by fitting the

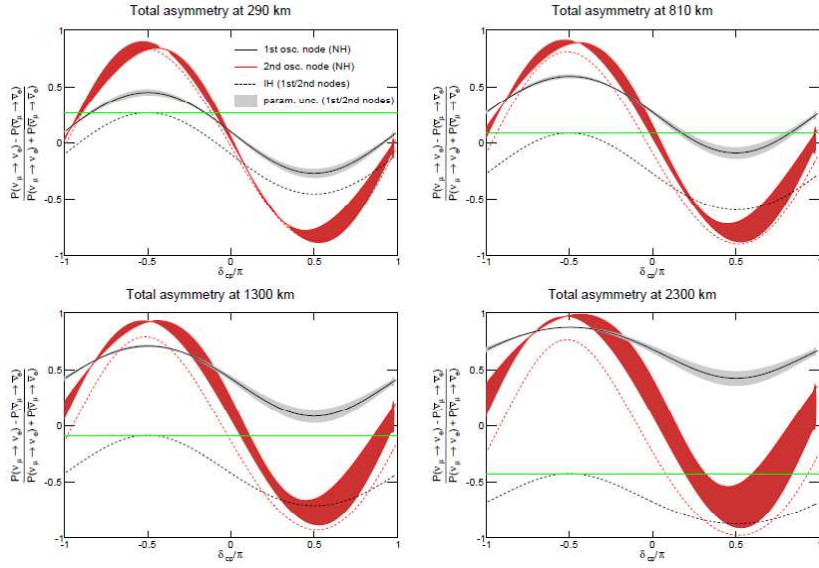


Figure 2.3: Total \mathcal{A}_{CP} as a function of δ_{CP}/π for four different baselines (290km, 810km, 1300km and 2300km). The black (red) lines indicate the asymmetries at the first (second) node, the full ones being for NH and the dashed ones for IH. [47]

simulated oscillation spectra of $\nu_\mu \rightarrow \nu_{\mu,e}$ and $\bar{\nu}_\mu \rightarrow \bar{\nu}_{\mu,e}$ for different values of the oscillation parameters and confronting the results with the expected "true" theoretical values in terms of $\Delta\chi^2$:

$$\Delta\chi^2_{MO} = |\chi^2_{MH^{test}=IH} - \chi^2_{MH^{test}=NH}| \quad (2.16)$$

$$\Delta\chi^2_{CPV} = \min(\Delta\chi^2_{CP}(\delta_{CP}^{test} = 0), \Delta\chi^2_{CP}(\delta_{CP}^{test} = \pi)) \quad (2.17)$$

with $\Delta\chi^2_{CP} = \chi^2(\delta_{CP}^{test}) - \chi^2(\delta_{CP}^{true})$. The significance with which DUNE will be able to assess the mass ordering grows with the exposure , defined as $k t$ of active volume \times MW beam? s power \times years, and varies wildly with the value of δ_{CP} (Fig.2.4). In order to ensure the DUNE objective of reaching $\sqrt{\Delta\chi^2} = 5$ for every value of δ_{CP} approximately an exposure of 200-400 $k t \times MW \times years$ will be need. The significance for δ_{CP} similarly grows with exposure (Fig.2.6), but only for values different from 0 and π , for which there is no CP violation and $\sqrt{\Delta\chi^2} = 0$ always. The significance for both MO and CPV also depends strongly on the values of all the oscillation parameters (Fig. 2.5 and 2.7), making precision measurements with DUNE mandatory.

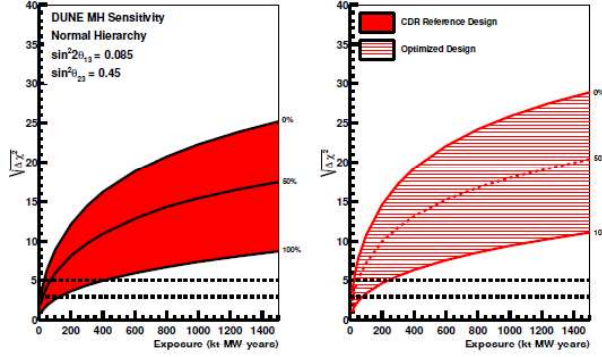


Figure 2.4: MO significance as a function of exposure for two different beam designs (left and right) and three values of CP asymmetry (0%, 50%, 100%). [47]

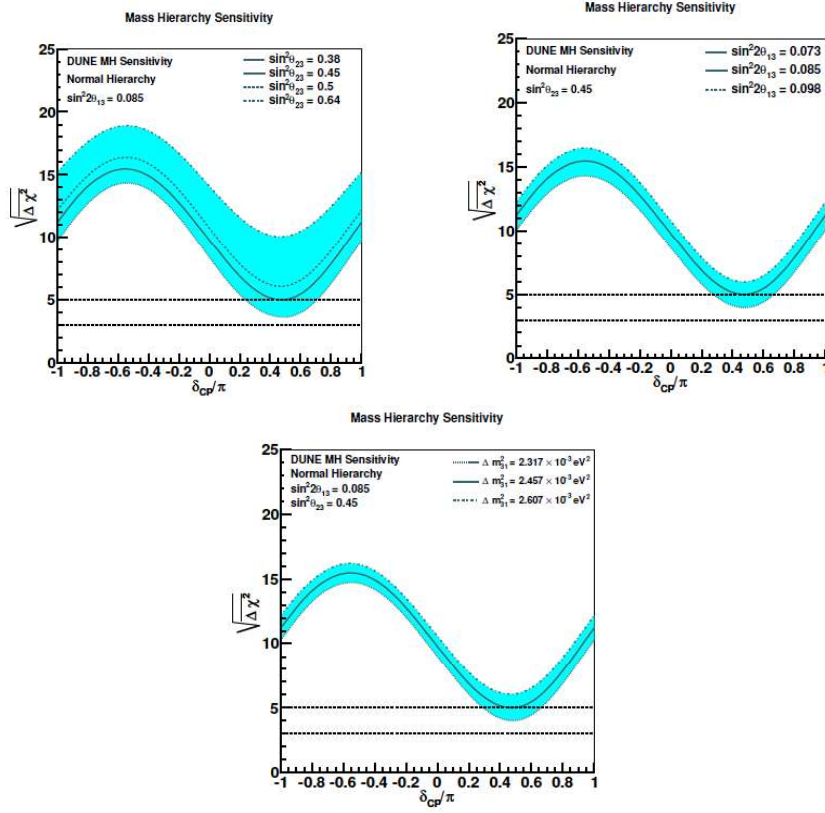


Figure 2.5: MO significance as a function of δ_{CP}/π at a fix value of exposure 300 kt \times MW \times years for different values of the oscillation parameters: θ_{23} (upper-left), θ_{13} (upper-right), δm_{31}^2 (bottom) [47]

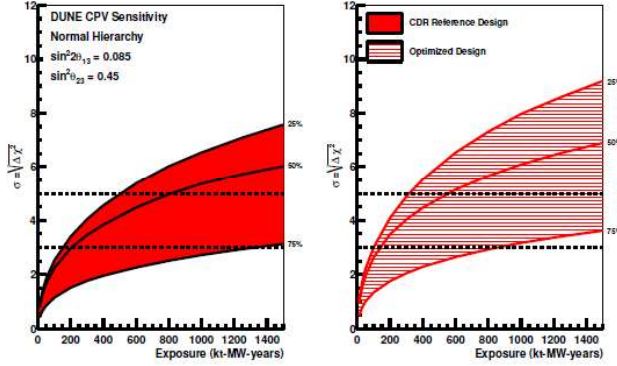


Figure 2.6: CPV significance as a function of exposure for two different beam designs (left and right) and three values of CP asymmetry (0%, 50%, 100%). [47]

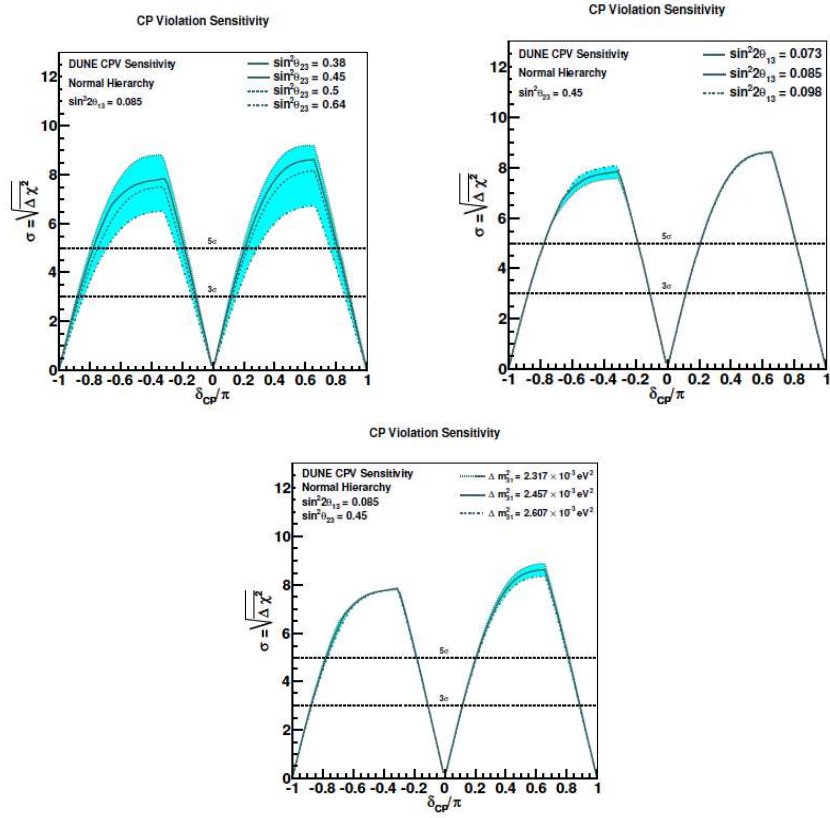


Figure 2.7: CPV significance as a function of δ_{CP}/π at a fix value of exposure 300 $kt \times MW \times years$ for different values of the oscillation parameters: θ_{23} (upper-left), θ_{13} (upper-right), Δm_{31}^2 (bottom) [47]

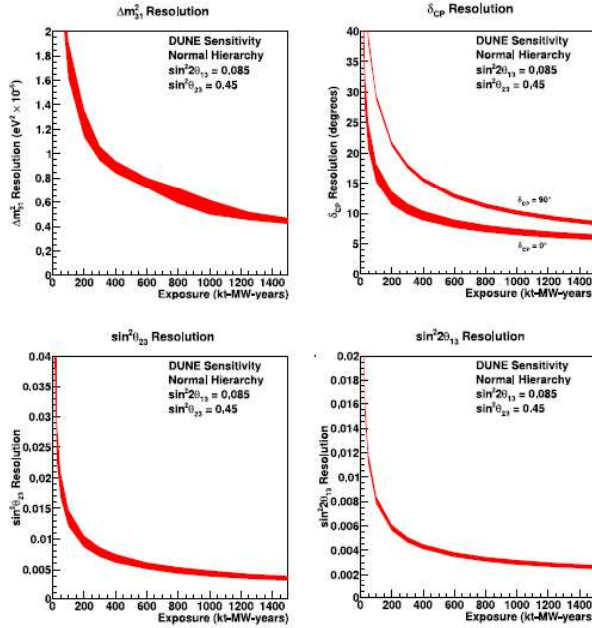


Figure 2.8: Resolution as a function of exposure for Δm_{31}^2 (upper left), δ_{CP} (upper right), $\sin^2 \theta_{23}$ (bottom left) and $\sin^2 \theta_{13}$ (bottom right). The red area represents the range in sensitivity due to differences in beam design. [47]

2.1.3 Precision Measurements

The DUNE experiment will improve sensitivity on the key parameters governing $\nu_1 - \nu_2$ and $\nu_2 - \nu_3$:

- $\sin^2 \theta_{23}$ and the octant of θ_{23} ;
- δ_P ;
- $\sin^2 \theta_{13}$;
- Δm_{31}^2 .

The sensitivity to these parameters as a function of exposure is plotted in Figure 2.8

Determining the octant of the mixing angle θ_{23} , and thus if its value is exactly 45° producing maximal mixing between mass eigenstates 2 and 3 $\sin^2 \theta_{23}$ is still an open question, with the latest results from T2K leaving both a lower ($< 45^\circ$) and upper ($< 45^\circ$) octant scenarios open, depending on the mass hierarchy being considered. This particular question is of great theoretical interest. A value of θ_{23} being exactly 45° would hint at new nt yet considered

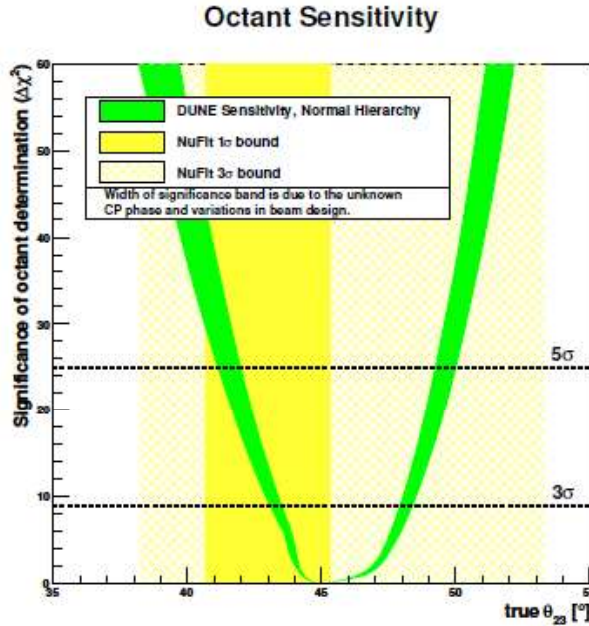


Figure 2.9: $\Delta\chi^2_{octant}$ as a function of θ_{23} . The yellow areas indicate the 1σ and 3σ intervals for the value of θ_{23} from recent global fits. The green area represents the range in sensitivity due to differences in beam design and δ_{CP} value.[46]

symmetries, while for example an excess in the upper octant of the order of the Cabibbo angle, point in the direction of quark-lepton universality models. The measurement of the octant is made possible by combining survival ($\nu_\mu \rightarrow \nu_\mu$) and oscillation ($\nu_\mu \rightarrow \nu_e$) probabilities, the first being sensitive to $\sin^2 2\theta_{23}$ and the second to $\sin^2 \theta_{23}$. The $\Delta\chi^2$ for the determination of the octant is then:

$$\Delta\chi^2_{octant} = |\chi^2_{\theta_{23}>45^\circ} - \chi^2_{\theta_{23}<45^\circ}| \quad (2.18)$$

The sensitivity to the octant as a function of θ_{23} is plotted in Fig.2.9. DUNE will also be able to perform unitarity tests of the PMNS matrix by measuring precisely the value of $\sin 2\theta_{13}$, which will constrain the phase space of possible new physics. In general the high precision measurement performed by dune could reveal new physics driven for example by non-standard interactions or the existence of sterile neutrinos.

2.1.4 Proton decay measurements

Almost all Grand Unified Theories (GUTs) predict some sort of proton decay and baryon number non conservation. Detecting a proton decay would

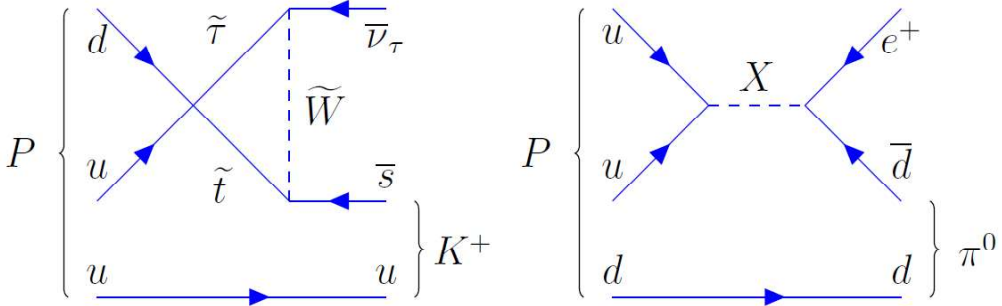


Figure 2.10: Feynman diagrams for two major proton decay modes: the main decay for SUSY GUTs $p^+ \rightarrow K^+ \bar{\nu}$ (left) and the main decay for gauge-mediation GUTs $p^+ \rightarrow e^+ \pi^0$ (right)[46]

be in fact one of the only viable experimental strategies to probe these theories since the unification scale is in excess of about 10^{15} GeV with respects to energies accessible to accelerator experiments. Early GUT theories were in fact one of the main motivations behind the construction of underground kt-scale experiments such as Kamiokande, as already mentioned in Section 1.4. The non-detection of proton decay set proton life-time constraints and progressively rule out theories based on their predictions. The most recent limits set by Super-Kamiokande have in fact confirmed the ruling out of minimal SU(5) (previously established by IMB and Kamiokande) and has disproved minimal SUSY SU(5). The next generation of large underground experiment such as Hyper-Kamiokande and DUNE will be well equipped to continue the search and, at the very least, make the constraints more stringent.

From the theoretical body of work, two main decay mode emerge, the first from supersymmetric GUTs and the second from gauge-mediated GUTs (see Fig. 2.10 for the Feynmann diagrams):

$$p^+ \rightarrow K^+ \bar{\nu} \quad (2.19)$$

$$p^+ \rightarrow e^+ \pi^0 \quad (2.20)$$

The first decay mode is especially interesting for large LArTPCs (such as the FD of DUNE) since it presents a kaon in its final state: kaons have an especially high ionization rate and would be detected with great efficiency using liquid Argon technologies. The second one is perhaps better known and has its most clear signature in Cherenkov detectors, since it consists of an electromagnetic shower ignited by the the e^+ and two γ from the π^0 decay.

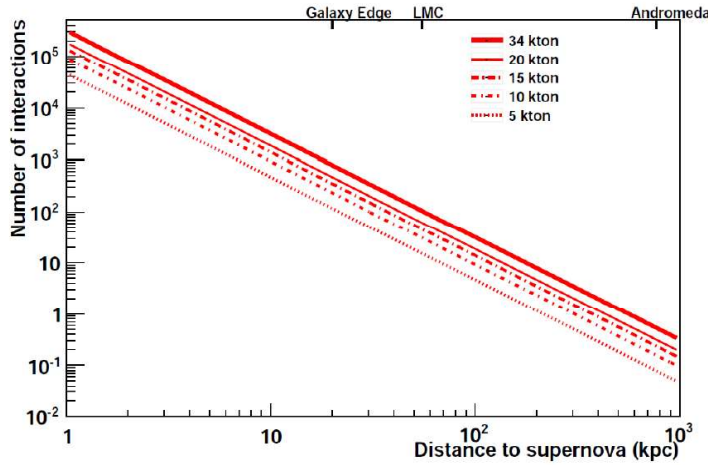


Figure 2.11: Number neutrino interactions from supernova explosions, as a function of distance, for different volume LArTPCs.[46]

2.1.5 Supernova neutrino measurements

Given an experimental life of 20 years, DUNE would have about a 40% chance of observing neutrinos from a core collapse Supernova in the Milky Way. This would be of great importance for our understanding of this astrophysical phenomenon, which as of now only been confirmed in its basic characteristics by the observation of neutrino events from SN1987, a supernova in the Large Magellanic Cloud, 50 kpc away.

Supernovas also promise an extremely varied environment to study neutrino oscillation, with their initial flavour composition being strictly linked to the expanding shock and turbulence. For example the oscillation patterns would be very different for NH and IH ;the oscillations of neutrinos and anti-neutrinos would also manifest rather differently, making the observation of both with high statistics of particular interest.

While water Cherenkov detectors are more sensitive to $\bar{\nu}_e$, LArTPCs are primarily sensitive to ν_e , making them complementary in Supernova detection. The unique sensitivity to electron neutrinos of Argon detectors is due to the absorption channel on Argon:



This interaction can be in principle detected exploiting the coincidence of the gamma cascade produced by the de-excitation of ${}^{40}\text{K}^*$ and the electron. The plot in Figure 2.11 shows the number neutrino interactions from supernova explosions, as a function of distance, for LArTPCs of different volumes. For

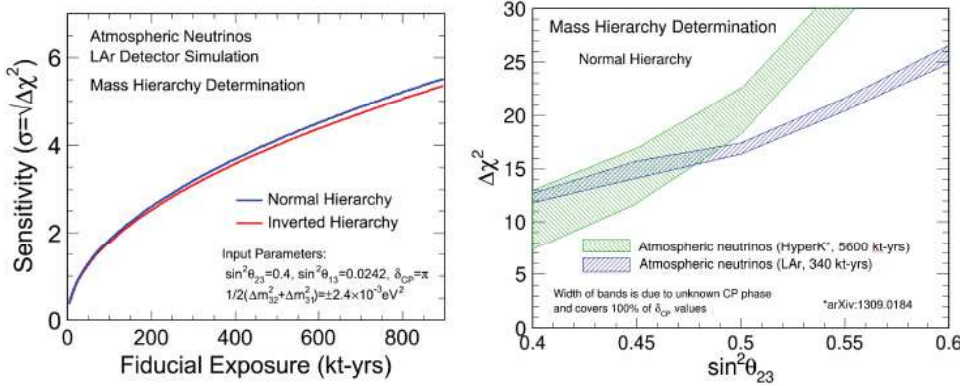


Figure 2.12: (*Left*) MO sensitivity for the atmospheric neutrino sample as a function of exposure for both NH (blue) and IH (red); (*Right*) MO sensitivity for the atmospheric neutrino sample as a function of the true value of θ_{23} in NH, with values for Hyper-K given for comparison.[48]

a detector of 10 kt, about the size of the FD of DUNE, a Supernova explosion at the likely distance of about 10 kpc would produce about 900 events. Only 19 events from two Cherenkov detectors and a few more from scintillation detectors were registered for SN1987A.

2.1.6 Oscillation physics with atmospheric neutrinos

DUNE's Far Detector, given its 10kt volume and being ~ 1500 m underground (sufficient for cosmic ray shielding), will be well equipped to do oscillation measurements using atmospheric neutrinos. Given that the atmospheric sample contains ν 's of all flavours over a vast range of energy and path length including some for which matter effects are relevant, all oscillation parameters could be measured, offering a very useful complementary program to the main accelerator one.

Measuring atmospheric oscillations would also be very useful in the field of mass ordering determination. The MO sensitivity , using the atmospheric neutrino sample, goes as the square root of the exposure and is thus not limited by systematics. Additionally it is dependent on the value of $\sin^2 \theta_{23}$ offering an alternative method of measuring θ_{23} and its octant.

Finally, new physics searches are also possible in the atmospheric sector, with previous experiments having set limits on CPT violation, non-standard interactions, Lorentz-invariance violation and neutrino mass variance.

2.1.7 Near Detector Physics

The Near detector main goal will be to provide precision measurements necessary to take into account the systematic uncertainties typical of a long baseline neutrino experiments. These measurements include the characterization of the neutrino flux and its energetic spectrum and flavour composition, which is mandatory to make predictions on the far/near flux ratio. It will also measure the secondary hadrons produced in NC and CC interactions, which are the dominant component of the oscillation background.

Since the near detector will be subjected to a high statistic of neutrino interactions it will also have an independent program, focused on flux measurements of fluxes, cross sections and particle production over a wide energetic range (0.5-50 GeV). Of particular importance will be the evaluation of the neutrino-Argon cross section and the characterizations of the various interaction channels.

Finally the large samples of events to which the Near Detector will be subjected can be exploited for sensitive studies in the electroweak sector and the search for new physics. Some of these endeavours can include for example the search for heavy sterile neutrinos with large oscillation Δm^2 of the order of 1 eV², for which some indications already exist. The ND will also be able to look for light dark matter WIMP-like particles. These could be distinguished from neutrino signatures by using timing information, assuming that the WIMPS are much heavier than the neutrinos and travel slower through matter, and spacial informations.

2.2 LBNF/DUNE's facilities and design

The experimental facilities and detectors will be divided between the Long-Baseline Neutrino Facility (LBNF), hosted by Fermilab and the DUNE collaboration. The first will provide the facilities in Illinois (Near Detector Facilities) and South Dakota at SURF (Far Detector facilities), necessary for the scientific program of DUNE. The collaboration will supervise the NuMI neutrino beam with the necessary upgrades, the ND conventional facilities in Fermilab and the construction of the caverns necessary to host the four liquid Argon far detectors. The DUNE collaboration will overview the design and construction of the detectors themselves. [50]

2.2.1 FD reference design: single phase LArTPC

The reference design for DUNE's Far Detector consists of four 10 kt single-phase Liquid Argon Time projection chambers (for a total fiducial mass of

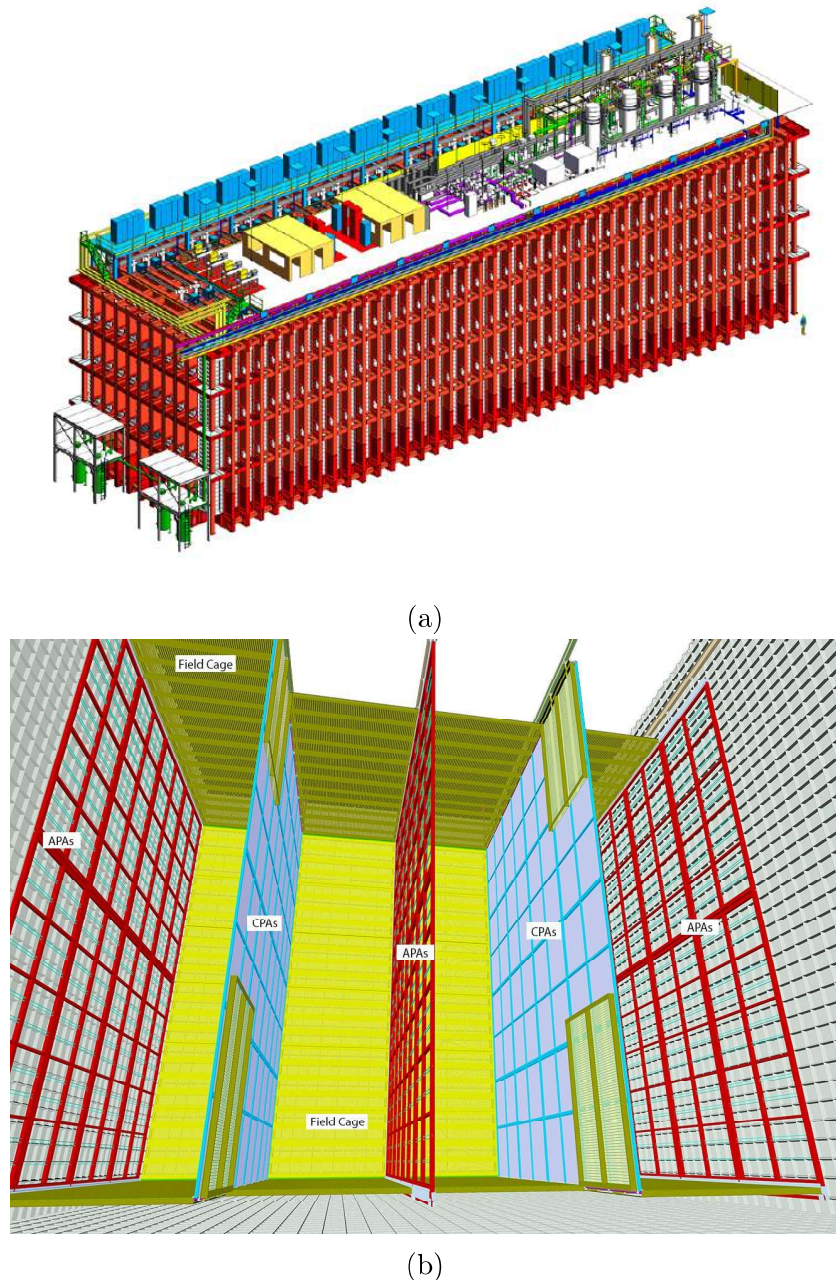


Figure 2.13: 3D Model of the FD single-phase reference design seen from outside (a) and inside of the TPC (b) [50]

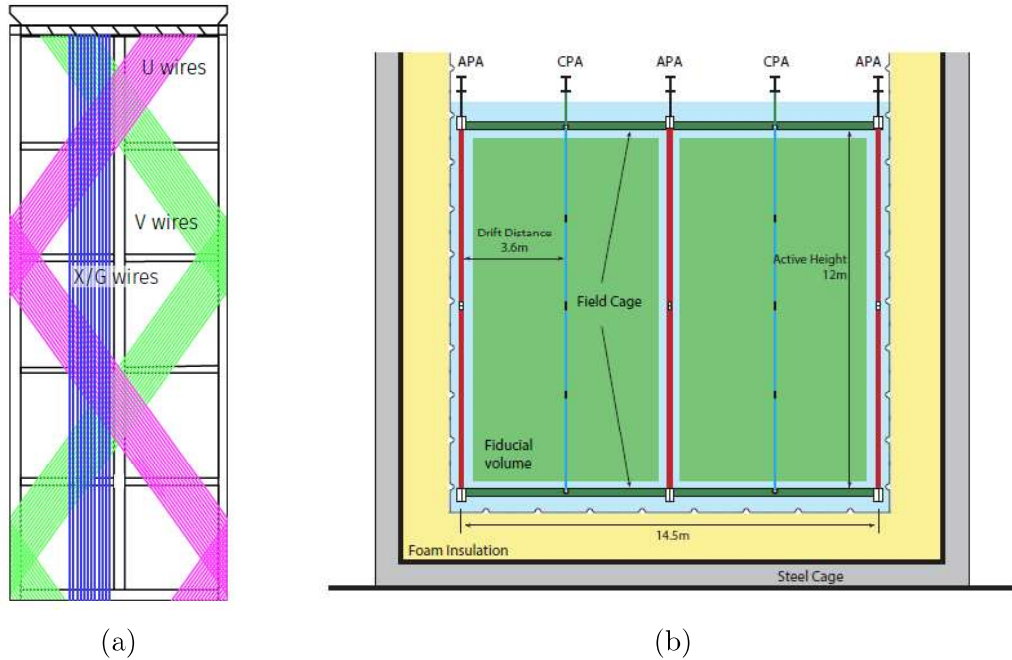


Figure 2.14: (a) Wiring scheme of an APA module (b) Front schematic view of the inside of the TPC [50]

40kt), each suspended inside a cryostat and augmented with a photon detection system (A model of the reference design is shown in Fig 2.13).

The LArTPC technology will be extrapolated from the pioneering techniques used by ICARUS. The charged particles in liquid Argon (LAr) produce ionization and scintillation light. The electrons drifting from the cathode plane towards the segmented anode plane produce a signal then used to provide spatial information. The prompt scintillation photons are collected by a photon detection system that provide the absolute timing of the event. In particular a detector is single-phase if the ionization, drift and collection all occur in Liquid Argon.

The two main active components of the detector are then the actual Time Projection Chamber (TPC) and the Photon Detection System (Photon Detector System), with the electronics divided in Cold Electronics (CE), mounted inside the Liquid Argon TPC, and the rest of the Data Aquisition System (DAQ).

The Time Projection Chamber (TPC)

The TPC is the fundamental detector of DUNE's FD design. It is located inside an external cryostat keeping its temperature at 88 K (necessary

Label	Function	Orientation (from vertical)	Pitch (mm)	Number	Bias Voltage (volt)
G	Shield/grid plane	0°	4.79	960	-655
U	1 st induction plane	+35.7°	4.67	800	-365
V	2 nd induction plane	-35.7°	4.67	800	0
X	Collection plane	0°	4.79	960	+860

Table 2.15: Bias voltage, orientation and pitch of the APA wire layers [50]

to keep the Argon in its liquid phase) and is built modularly from anode plane assemblies (APA), cathode plane assemblies (CPA) and field cage modules. The APAs and CPAs are assemblies of wire planes and are placed in rows, parallel to the beam direction, to form three anode planes and two cathode planes respectively. Each anode plane is made of 25 vertical stacks of two 6m high and 2.3m wide APAs, while the cathode planes are equal in total size but double the number of CPAs, which are half the height of the anodic assemblies. The field cage modules close the four open sides left between the alternating vertical planes with the total structure being 12m high, 14.5m wide and 58 m long. A "slice" of the TPC, perpendicular to the beam direction, is shown in Figure 2.14 (b).

The APAs are built on each side of a lightweight rectangular frame and include four wire layers: from outside a shielding plane (G), two induction planes (U and V) and the collection plane (X). The CE front-end electronics are mounted directly on the module's frame. The wiring scheme is shown in Figure 2.14 (a).

The APAs and CPAs are set to a specific voltage so that an electric field, kept uniform by the field cage, is formed perpendicularly between the planes. When a charged particle traverses the chamber, it then forms a trail of ionized electrons and ions: these will then start drifting in opposite directions following the field lines. The electrons will drift towards the closest anode planes inducing an electric current signal in the electronics. The maximum electron-drift distance is set to 3.6m by applying a bias voltage to the cathodes of -180kV in order to obtain a nominal drift field of 500 V/cm. Note that each APA's wire layer is set to a specific voltage so that the ionization electrons drift past the first three and are collected exclusively in X (Table 2.15).

The waveforms are then digitized and sent through cold-resisting cables to the DAQ outside the cryostat. The DAQ system is designed to have high uptime of data collection (> 99%) for all types of interactions the detector is

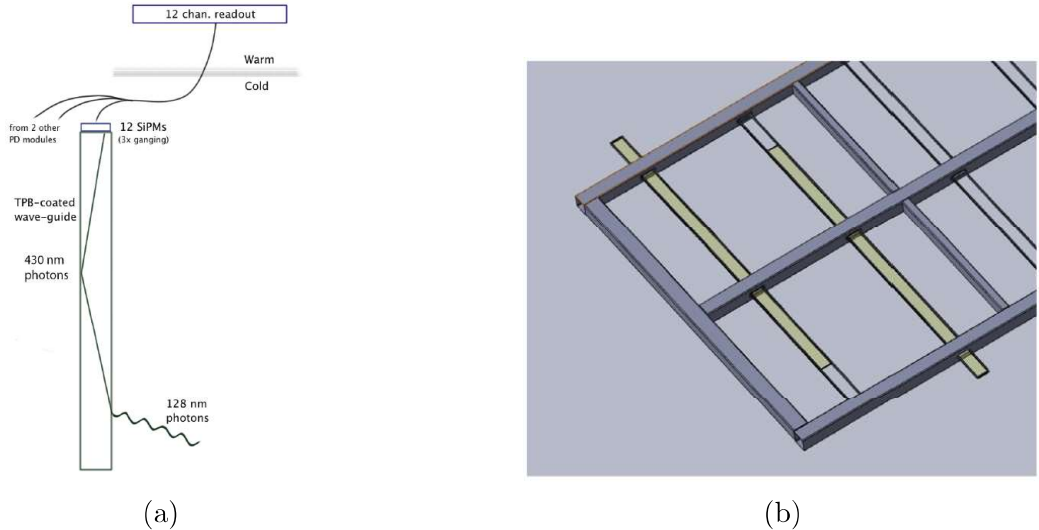


Figure 2.16: (a) Schematic representation of a PD module from the reference design (b) Positioning of the reference PD modules in the APA frame [50]

trying to detect: beam and atmospheric neutrino and proton decay products. The DAQ of each 10kt module is for this reason left independent reducing dead-time significantly.

Photon Detection System

A charged particle depositing 1 MeV in LAr will generate on average 40000 photons of wavelength roughly 128 nm,(VUV) to which the liquid Argon medium is highly transparent. About a fourth of them will be prompt photons emitted almost immediately (average lifetime ~ 6 ns), with the rest being emitted after 1100-1600 ns. The high light-yield makes the scintillation process ideal for determining the t_0 of non-beam related events, such as proton decay candidates and supernova or atmospheric neutrinos.

The reference Photon Detection system consists of modules to be mounted on the APA frames (Figure 2.16). They would consist of a light-guide and 12 Silicon Photo-multipliers (SiPM). The light-guide bar is painted with a wavelength shifter peaked at 430 nm, in order to match the maximum efficiency of the SiPMs. Each APA would host ten PD modules, positioned at equispaced intervals along the length of the anode module, each being 2.2 m in length, 83 mm wide and 6 mm thick.

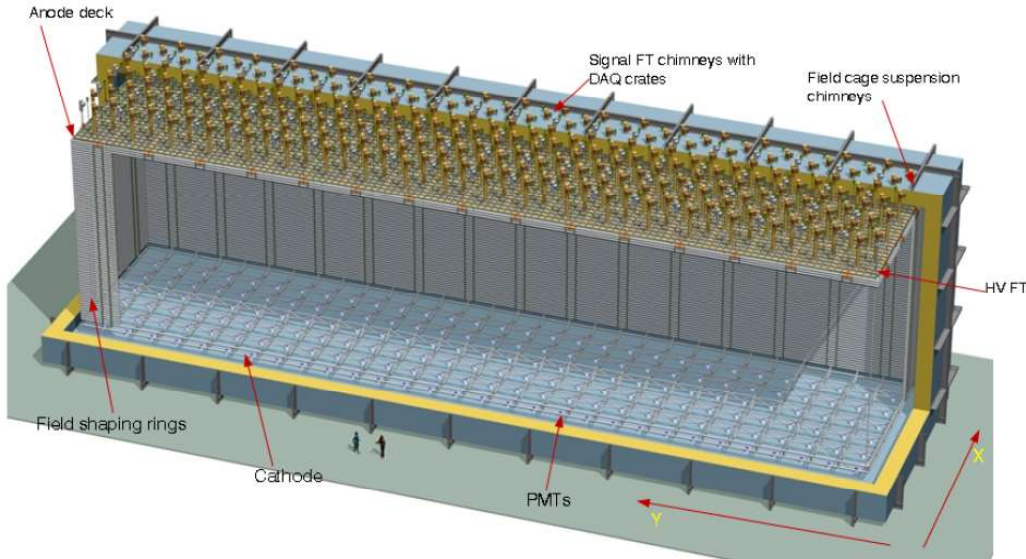


Figure 2.17: 3D model of the dual-phase LArTPC alternative design [50]

2.2.2 FD alternative design: double phase LArTPC

In addition to the reference design, which has already been chosen as the model for the first FD module, an alternative dual phase design, augmented with a light collection system, is being considered for the other three. In a dual phase LArTPC, the ionization electrons are produced in a tank filled with fully homogenous liquid argon, then drifted upwards towards an extraction grid just below a gaseous argon volume. They are then extracted, amplified via Townsend multiplication and finally collected on a finely segmented anode. This sort of design has several advantages, such as a generally higher gain and consequently a better signal to noise ratio (S/N), a larger fiducial volume and longer drift path and a lower detection threshold.

A 100 % extraction efficiency is achieved applying a 2kV/cm electric field between the extraction grid (made of stainless steel wires, 1mm in diameter and spaced by 3.125mm) and the amplification devices placed in ultra pure Argon gas. These devices, called Large Electron Multipliers (LEMs) are 1mm circuit boards placed between two electrodes, micro-patterned with tiny holes. Between the electrodes electron avalanches are induced by applying a 3kV potential difference. It is this feature in particular that improves the S/N ratio by at least an order of magnitude and lowers the threshold for energy deposition, improving resolution. The 2D finely segmented collection anode is placed on top of the gas phase volume and is connected to the first level of electronics.

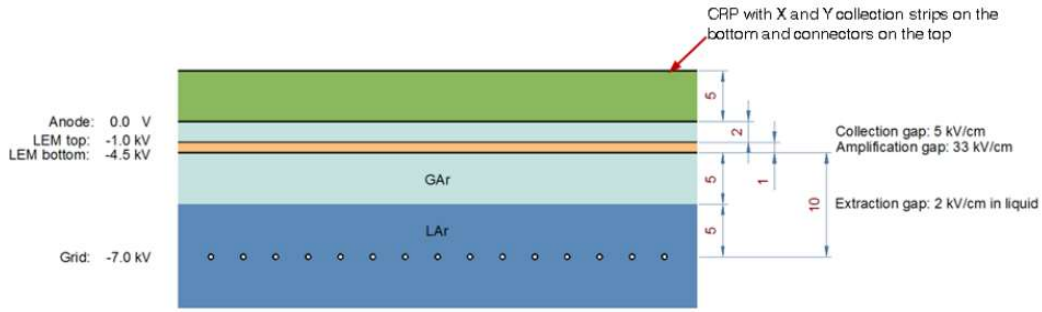


Figure 2.18: Schematic representation of a CRP module with thickness and voltage values for a 0.5 kV/cm drift field in liquid Argon. [50]

The collection grid, LEM and anode elements are segmented in $0.5 \times 0.5\text{m}^2$ sections and combined to form independent modules called Charge readout PLANES (CRPs), which are embedded in a FR-4 and stainless steel armour. These are suspended from the roof of the tank and cover the entire upper surface. Combined with PMT arrays, collecting the scintillation light for timing information, a CRP module provides 3D position and calorimetric reconstruction. A schematic representation of these elements is shown in Figure 2.18.

The cathode layer, to which the high voltage that produces the drift field ($E_{drift} \sim 0.5 \text{ kV/cm}$) covers the tank's floor. The field is kept homogenous by a field-cage, comprised of a stack of 60 field-shaping electrodes of decreasing voltage from bottom to top. The design is completed by the external cryostat and signal feed-through elements called chimneys, which put in contact the internal electronic with the outside of the tank. A 3D module of the entire structure is shown in Figure 2.17.

2.2.3 LBNF Beamline

The LBNF BeamLine at Fermilab is a horn-focused, sign-selected neutrino beam, designed to meet the DUNE's long-baseline physics requirements [49]. It is aimed towards the South Dakota facilities hosting the Far Detectors, 1480m underground and 1300 km away from the FNAL facilities.

The main components of the beamline are shown in Figure 2.19. A primary beam of accelerated protons (60-120 GeV) is produced in the Fermilab Main Injector (MI) (the primary beam main specifications and characteristics for 12 GeV protons are listed in Table 2.1). It is then extracted and transported through a man-made hill, at the apex of which it is bent downwards, toward a target at ground level, in the LBNF Target Hall. The total bend amounts

Parameter	Value
Energy	120 GeV
Protons per cycle	7.5×10^{13}
Spill duration	1.0×10^{-5} s
POT per year	1.1×10^{21}
Cycle Time	1.2 s
Beam Power	1.2 MW
Beam size at target	1.5-1.7 mm
$\Delta p/p$	11×10^{-4} 99% (28×10^{-4} 100%)
Transverse emittance	$30\pi \mu m$ 99% ($360\pi \mu m$ 100%)
Beam divergence (x,y)	15-17 μrad

Table 2.1: Summary of the main primary proton beam parameters [49]

to 7.2° westward and 5.4° downwards and directs the flux toward the Far Detectors.

When the accelerated protons hit the target, mesons are generated; these are then focused by magnetic horns into a decay pipe where they decay into muons and neutrinos. The decay pipe is 194 m long in total, with an additional 27 m acting as the target chase. The focusing structure, consisting of the two NuMI horns (placed 6.6m apart and set at 230 kA), provides neutrinos in the energy range 0.5-5 GeV range, which is enough to cover the first

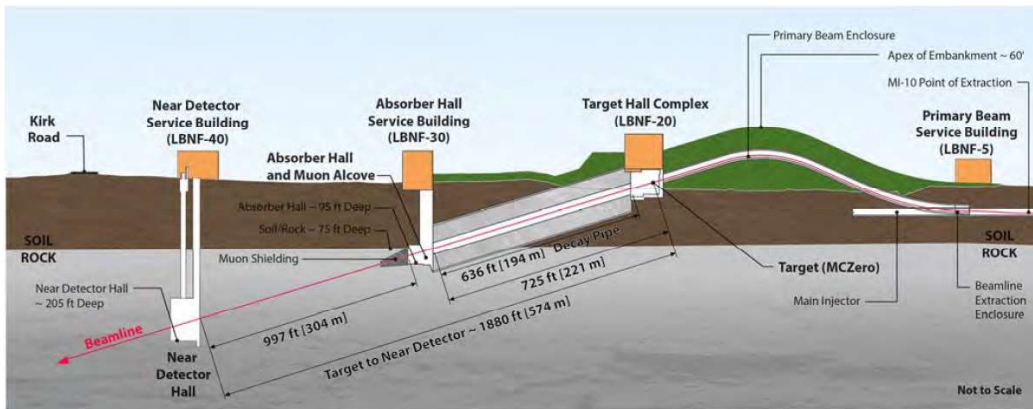


Figure 2.19: Schematic representation of the LBNF neutrino beamline facilities at Fermilab [49]

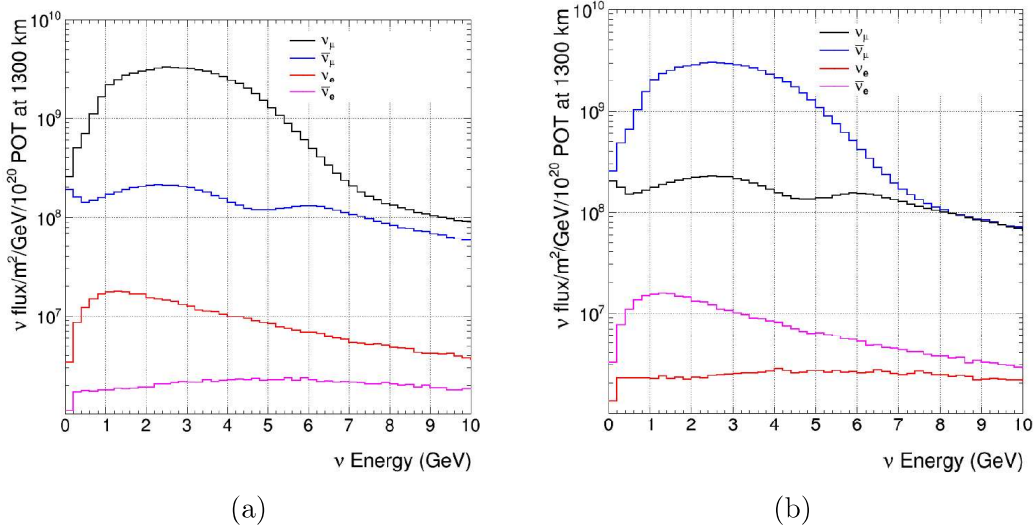


Figure 2.20: Expected neutrino and antineutrino beam produced focusing positive (a) and negative (b) mesons. [49]

two oscillation nodes (for a 1300 km baseline 2.4 and 0.8 GeV respectively). The facility is set to run initially with a power of 1.2 MW (later upgrading to 2.4MW), corresponding to 1.1×10^{21} protons-o-target (POT) per year, for 120 GeV protons. This assuming that 7.5×10^{13} protons are produced for each 1.2 s MI cycle and a total efficiency of 0.56 for the entire focusing and transportation in LBNF.

The neutrino and antineutrino expected fluxes obtained focusing positive and negative particles are shown in Figure 2.20.

2.2.4 The Near Detector

The near detector will be located in the Fermilab facilities a few hundred meters away from the NuMI beam source. It will constitute of a movable system, capable of being positioned both on and off-axis, and a fixed one that will always be on axis. The movable detector doesn't have yet a complete design, but the physics' program necessities require that it will contain a LArTPC, an electronic calorimeter (ECAL), a central tracker and a muon identifier.

The fixed detector will reuse parts of a previous detector named KLOE, today situated at the Laboratori Nazionali di Frascati (LNF). It will take the name SAND and its current design and purpose will be the topic of the next chapter.

Chapter 3

SAND

Bibliography

- [1] W. Pauli, "Letter to a physicist's gathering at Tübingen", December 4, 1930. Reprinted in Wolfgang Pauli, Collected Scientific Papers, ed. R. Kronig and V. Weisskopf, Vol. 2, p. 1313 (Interscience: New York, 1964).
- [2] E. Fermi, "Tentativo di una Teoria Dei Raggi β ", Il Nuovo Cimento, vol. 11, pp. 1-19, Jan 1934
- [3] H. Bethe and R. Peierls, "The neutrino", Nature, vol. 133, p. 532, 1934
- [4] B. Pontecorvo, "Inverse beta process" Camb. Monogr. Part. Phys. Nucl. Phys. Cosmol., vol. 1, pp. 25-31, 1991.
- [5] F. Reines and C. L. Cowan, "The neutrino" Nature, vol. 178, pp. 446-449, Sep 1956.
- [6] G. Danby, J. M. Gaillard, K. A. Goulian, L. M. Lederman, N. B. Mistry, M. Schwartz, and J. Steinberger, "Observation of High-Energy Neutrino Reactions and the Existence of Two Kinds of Neutrinos", Phys. Rev. Lett., vol. 9, pp. 36-44, 1962.
- [7] ALEPH Collaboration, D. Decamp et al., Phys. Lett. B 235, pp. 399, 1990
- [8] DONUT Collaboration, K. Kodama et al., Phys. Lett. B 504, pp. 218-224, 2001.
- [9] P. Lipari, "Introduction to neutrino physics", chapter 13: "Models for neutrino masses" in 2001 CERN-CLAF School of high-energy physics, Itacuruca, Brazil, 6-19 May, 2001: Proceedings, pp. 115-199, 2001.
- [10] S. T. Petcov, "The Nature of Massive Neutrinos", Adv. High Energy Phys., vol. 2013, p. 852987, 2013.

- [11] V. N. Aseev et al., "An upper limit on electron antineutrino mass from Troitsk experiment", Phys. Rev., vol. D84, p. 112003, 2011
- [12] C. Kraus et al., "Final results from phase II of the Mainz neutrino mass search in tritium beta decay", Eur. Phys. J., vol. C40, pp. 447?468, 2005.
- [13] Aker 2019, "Improved Upper Limit on the Neutrino Mass from a Direct Kinematic Method by KATRIN", 123, 1079-7114, Physical Review Letters, American Physical Society (APS), Aker, M. and Altenmüller, K. and Arenz, M. and Babutzka, M. and Barrett, J. and Bauer, S. and Beck, M. and Beglarian, A. and Behrens, J. and Bergmann, T. and et al. 2019 Nov
- [14] M. Tanabashi et al., "Review of particle physics", Phys. Rev. D, vol. 98, p. 030001, Aug 2018.
- [15] K. Zuber, Neutrino Physics, Second Edition. Aug. 2011.
- [16] C. Giunti and C. W. Kim, Fundamentals of Neutrino Physics and Astrophysics. 2007.
- [17] L. Wolfenstein, Phys. Rev. D17 (1978) 2369; S.P. Mikhaev and A.Y. Smirnov, Sov.J.Nucl.Phys. 42 (1985) 913; S.P. Mikhaev and A.Y. Smirnov, Nuovo Cimento C9 (1986) 17.
- [18] Stefania Ricciardi, "Lecture notes on Neutrino oscillations in matter", 6/10/2013
- [19] J. N. Bahcall, M. H. Pinsonneault, and S. Basu, "Solar models: Current epoch and time dependences, neutrinos, and helioseismological properties", Astrophys. J., vol. 555, pp. 990?1012, 2001,
- [20] K. Lande and P. Wildenhain, "The homestake chlorine solar neutrino experiment?past, present and future", Nuclear Physics B - Proceedings Supplements, vol. 118, pp. 49?54, Apr 2003.
- [21] J. N. Abdurashitov, E. P. Veretenkin, V. M. Vermul, V. N. Gavrin, S. V. Girin, V. V. Gorbachev, P. P. Gurkina, G. T. Zatsepин, T. V. Ibragimova, A. V. Kalikhov, and et al., "Solar neutrino flux measurements by the soviet-american gallium experiment (sage) for half the 22-year solar cycle", Journal of Experimental and Theoretical Physics, vol. 95, pp. 181?193, Aug 2002.

- [22] M. Altmann and Others, "Complete results for five years of gno solar neutrino observations", Physics Letters B, vol. 616, no. 3, pp. 174 ? 190, 2005.
- [23] Y. Suzuki, "The super-kamiokande experiment", The European Physical Journal C, vol. 79, Apr 2019.
- [24] Q. R. Ahmad et al., "Direct evidence for neutrino flavor transformation from neutral current interactions in the Sudbury Neutrino Observatory", Phys. Rev. Lett., vol. 89, p. 011301, 2002, nuclex / 0204008.
- [25] S. Abe, T. Ebihara, S. Enomoto, K. Furuno, Y. Gando, K. Ichimura, H. Ikeda, K. Inoue, Y. Kibe, Y. Kishimoto, and et al., "Precision measurement of neutrino oscillation parameters with kamland",Physical Review Letters, vol. 100, Jun 2008.
- [26] G. Alimonti and Others, "The borexino detector at the laboratori nazionali del gran sasso", Nuclear Instruments and Methods in Physics Research Section A: Accelerators, Spectrometers, Detectors and Associated Equipment, vol. 600, pp. 568?593, Mar 2009.
- [27] Valle, José Wagner Furtado, and Jorge Romao. "Neutrinos in High Energy and Astroparticle Physics", John Wiley & Sons, Incorporated, 2055
- [28] F. An and Others, "Measurement of electron antineutrino oscillation based on 1230 days of operation of the daya bay experiment", Physical Review D, vol. 95, Apr 2017
- [29] S.-B. Kim, "New results from reno and prospects with reno-50", Nuclear and Particle Physics Proceedings, vol. 265-266, pp. 93?98, Aug 2015.
- [30] J. I. Crespo-Anadón, "Double Chooz: Latest results," Nucl. Part. Phys. Proc., vol. 265- 266, pp. 99?104, 2015.
- [31] Y. Farzan and M. Tortola, "Neutrino oscillations and Non-Standard Interactions", Front.in Phys., vol. 6, p. 10, 2018.
- [32] Y. Ashie et al., "A Measurement of atmospheric neutrino oscillation parameters by SUPERKAMIOKANDE I," Phys. Rev., vol. D71, p. 112005, 2005, hep-ex/0501064.
- [33] W. W. M. Allison et al., "Measurement of the atmospheric neutrino flavor composition in Soudan-2", Phys. Lett., vol. B391, pp. 491?500, 1997.

- [34] G. Giacomelli, "Neutrino physics and astrophysics with the MACRO experiment at the Gran Sasso lab", *Braz. J. Phys.*, vol. 33, pp. 211?217, 2003.
- [35] S. Boyd, "Recent results from the k2k (kek-to-kamioka) neutrino oscillation experiment", *Nuclear Physics B - Proceedings Supplements*, vol. 98, pp. 175?181, Apr 2001.
- [36] J. Evans, "The MINOS Experiment: Results and Prospects", *Adv. High Energy Phys.*, vol. 2013, p. 182537, 2013.
- [37] N. Agafonova, A. Alexandrov, A. Anokhina, S. Aoki, A. Ariga, T. Ariga, A. Bertolin, C. Bozza, R. Brugnera, A. Buonaura, and et al., "Final Results of the OPERA Experiment on ν_τ Appearance in the CNGS Neutrino Beam", *Physical Review Letters*, vol. 120, May 2018.
- [38] F. Vannucci, "The nomad experiment at cern", *Advances in High Energy Physics*, vol. 2014, pp. 1?20, 2014.
- [39] A. G. Cocco, "Results from CHORUS experiment at CERN," *Phys. Rept.*, vol. 307, pp. 319?324, 1998.
- [40] C. Giganti, "Latest results from T2K and T2K Phase II," in *Proceedings, Prospects in Neutrino Physics (NuPhys2017)*: London, UK, December 20-22, 2017, pp. 61?69, 2018.
- [41] F. Jedny, "Nova latest results", *Proceedings of The 15th International Conference on Flavor Physics & CP Violation ? PoS(FPCP2017)*, Oct 2017.
- [42] W. Marciano and Z. Parsa, "Intense neutrino beams and leptonic CP violation", *Nucl. Phys. Proc. Suppl.*, vol. 221, pp. 166?172, 2011.
- [43] K. Abe et al., "Measurement of neutrino and antineutrino oscillations by the t2k experiment including a new additional sample of ν_e interactions at the far detector", *Phys. Rev. D*, vol. 96, p. 092006, Nov 2017.
- [44] I. Esteban, M. C. Gonzalez-Garcia, A. Hernandez-Cabezudo, M. Maltoni, and T. Schwetz, "Global analysis of three-flavour neutrino oscillations: synergies and tensions in the determination of θ_{23} ; δ_{CP} , and the mass ordering", *JHEP*, vol. 01, p. 106, 2019
- [45] F. Capozzi, E. Di Valentino, E. Lisi, A. Marrone, A. Melchiorri, and A. Palazzo, "Global constraints on absolute neutrino masses and their ordering", *Phys. Rev.*, vol. D95, no. 9, p. 096014, 2017.

- [46] C. Adams et al., "The Long-Baseline Neutrino Experiment: Exploring Fundamental Symmetries of the Universe", in Snowmass 2013: Workshop on Energy Frontier Seattle, USA, June 30-July 3, 2013.
- [47] R. Acciarri et al., "Long-Baseline Neutrino Facility (LBNF) and Deep Underground Neutrino Experiment (DUNE), Conceptual Design Report Volume 2: The Physics Program for DUNE at LBNF", 2015.
- [48] E. Kearns et al., "Hyper-Kamiokande Physics Opportunities", in Proceedings, 2013 Community Summer Study on the Future of U.S. Particle Physics: Snowmass on the Mississippi (CSS2013): Minneapolis, MN, USA, July 29-August 6, 2013.
- [49] R. Acciarri et al., "Long-Baseline Neutrino Facility (LBNF) and Deep Underground Neutrino Experiment (DUNE), Conceptual Design Report Volume 3: The Physics Program for DUNE at LBNF", 2015.
- [50] R. Acciarri et al., "Long-Baseline Neutrino Facility (LBNF) and Deep Underground Neutrino Experiment (DUNE), Conceptual Design Report Volume 4: The DUNE Detectors at LBNF", 2016.